JOURNAL OF GEOPHYSICAL RESEARCH, VOL. 93, NO. C1, PAGES 533–542, JANUARY 15, 1988

The Generation of Internal Waves by Tidal Flow Over Stellwagen Bank

TOSHIYUKI HIBIYA

Earthquake Research Institute, University of Tokyo, Japan

The generation mechanism of internal waves by tidal flow over Stellwagen Bank in Massachusetts Bay is qualitatively clarified. First, in order to demonstrate the continuous generation process of internal waves, a numerical simulation is carried out for the hydrographic condition during a field study by Chereskin (1983). The resulting internal waveforms agree well with the acoustic images obtained at several stages of the tidal flow. Next, the generation mechanism for these internal waves is analyzed via a physical interpretation of the calculated result. This analysis is made by use of characteristics which describe the propagation of the first- and second-mode internal waves. It is shown that each mode internal wave with an upstream phase propagation is efficiently amplified while being carried downstream toward the location where the maximum tidal flow becomes critical: with the decrease of the tidal flow, the internal wave thus amplified begins to propagate upstream. In previous studies, these internal waves were interpreted as quasi-steady lee waves. The present analysis, however, provides a satisfactory explanation for the time-dependent features that are shown in numerical simulation. This indicates that the internal waves over the bank are transient waves formed in response to a time-varying tidal flow, and not quasi-steady lee waves.

1. INTRODUCTION

There have been a number of reports on internal wave observations in various fields around the world; nevertheless, detailed observations made in the generation region which focus on the time dependent interaction between tidal flow and bottom topography are largely lacking. A few exceptions include the field study by *Farmer and Smith* [1980] over a large-amplitude sill in Knight Inlet and that by *Chereskin* [1983] over Stellwagen Bank in Massachusetts Bay. They demonstrated the existence of considerable spatial and temporal variability in the internal wave fields over topographic features by use of acoustic echo sounding systems. Chereskin, in particular, made simultaneous hydrographic observations of tidal flow velocity and vertical density stratification over the bank for the interpretation of the acoustic images. In both studies, these internal waves were interpreted as quasi-steady waves formed by a slowly varying tidal flow.

In an earlier paper [*Hibiya*, 1986], the author discussed the generation mechanism of internal waves by a relatively strong tidal flow over a sill. An analytical investigation by use of characteristics showed that an internal wave with an upstream phase propagation is gradually formed through the interference among infinitesimal-amplitude internal waves (elementary waves) emanated from the sill at each instant of time. It was also shown that effective amplification of the internal wave takes place as the Froude number exceeds (falls below) unity in the accelerating (decelerating) stage of tidal flow, because during this period, the internal wave slowly travels downstream (upstream) while crossing over the sill where elementary waves are efficiently superimposed. This generation mechanism is qualitatively consistent with several time dependent features that have been observed in laboratory studies [*Maxworthy*, 1979; *Lansing and Maxworthy*, 1984]. It is therefore suggested that these internal waves are transient waves formed in response to a time-varying tidal flow rather than quasi-steady waves. Although direct applicability of this theory to a large-amplitude topography is limited owing to the hypothesized linearized bottom boundary condition, a basic framework for the interpretation of field observations has been provided. As was mentioned above, in the case of Stellwagen Bank, simultaneous hydrographic observations of tidal flow and vertical stratification during the acoustic soundings of internal waves were carried out. Therefore it is possible to examine whether or not the acoustically observed variability in the internal wave field can be interpreted as the transient responses of stratified fluid.

In the present study, first, the continuous generation process of internal waves over Stellwagen Bank is demonstrated by means of a numerical simulation for the hydrographic condition during a field study by *Chereskin* [1983]. The result of this simulation is compared with the acoustic images obtained at several stages of the tidal flow. Next, the time dependent features of the internal wave generation are independently examined by use of characteristics [*Hibiya*, 1986]. Finally, the result of this theoretical analysis is compared with that of the numerical simulation to see whether or not the internal waves over the bank can be interpreted as transient waves formed in response to a time-varying tidal flow.

2. OBSERVATIONS

In this section, a brief description of the field study made by *Chereskin* [1983] is given.

The geographical location of Stellwagen Bank is shown in Figure 1, and the bathymetric cross section along line *G-H* in Figure 1 is shown in Figure 2. As can be seen in Figure 2, the bank's profile is markedly asymmetric: in contrast to a gentle seaward slope, a steep shoreward slope drops from 27 m to 80 m over a horizontal distance of roughly 1 km.

The bank has been under active field investigation [see *Haury et al.*, 1979, 1983; *Chereskin*, 1983] since *Halpern* [1971] suggested that tidal flow interaction with the above described profile might generate the high-frequency internal waves which were observed about 9 km shoreward of the bank in Massachusetts Bay. *Chereskin* [1983] conducted a detailed field observation in September 1979 to clarify the tidal phase of internal wave generation. The main tool used to monitor the isopycnal motion was a 41-kHz acoustic echo sounder which was operated while steaming continuously along the approximately 10-km track (line *G-H* in Figure 1). In fact, Chereskin compared isotherms contoured from an expendable bathy thermograph (XBT) section once made over the bank with a concurrent acoustic image and found corre-

Paper number 7C0838.
0148-0227/88/007C-0838$05.00

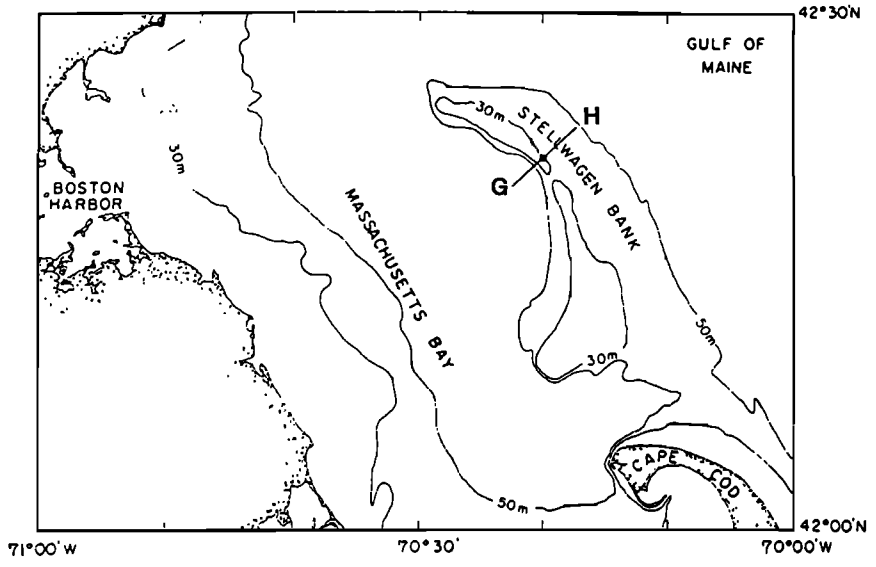

Fig. 1. Geographical location of Stellwagen Bank. Line *G-H* shows the steaming track along which the acoustic soundings of internal waves were made.

spondence between isothermal displacement and the acoustic backscattering. In addition to these acoustic soundings, simultaneous hydrographic observations of tidal flow velocity and vertical density stratification were made in the vicinity of the bank crest.

The tidal flow velocity was measured at half-hour intervals by current meters moored at three different depths. It was observed to be relatively independent of depth. A time series of the cross-bank component of the tidal flow velocity is shown in Figure 3. As is evident from the figure, the tidal flow over the bank is considerably distorted, and the ebb (seaward) tidal flow is about 2 times stronger than the flood (shoreward) tidal flow.

The vertical density stratification was measured during the field study on occasion with a hand-lowered conductivity-temperature-depth probe (CTD). The results (see Figure 3 in *Chereskin* [1983]) show that the ocean was continuously stratified, suggesting that the internal responses of higher modes might also be important over the bank.

3. Numerical Simulation

In order to demonstrate the continuous generation process of internal waves over Stellwagen Bank, a numerical simulation in the vertical two-dimensional plane defined in Figure 2 is carried out. Under the Boussinesq approximation, the equations of motion and continuity for an incompressible fluid can be written as

$$\frac{Du}{Dt} = -\frac{1}{\bar{\rho}_0}\frac{\partial p}{\partial x} + A_h\frac{\partial^2 u}{\partial x^2} + A_v\frac{\partial^2 u}{\partial z^2} \tag{1}$$

$$\frac{Dw}{Dt} = -\frac{1}{\bar{\rho}_0}\frac{\partial p}{\partial z} - \frac{\rho}{\bar{\rho}_0}g + A_h\frac{\partial^2 w}{\partial x^2} + A_v\frac{\partial^2 w}{\partial z^2} \tag{2}$$

$$\frac{D\rho}{Dt} = -w\frac{\partial \rho_0}{\partial z} \tag{3}$$

$$\frac{\partial u}{\partial x} + \frac{\partial w}{\partial z} = 0 \tag{4}$$

where t is time; u and w are the water velocities in the x and z directions, respectively; $D/Dt = \partial/\partial t + u(\partial/\partial x) + w(\partial/\partial z)$ is the total time derivative; ρ_0 is the water density in the undisturbed state; $\bar{\rho}_0$ is the mean of ρ_0; ρ is the water density perturbation; p is pressure; g is the acceleration due to gravity; and A_h and A_v are the coefficients of the horizontal and vertical eddy viscosity, respectively.

Introducing the stream function ψ defined by

$$u = \frac{\partial \psi}{\partial z}, \qquad w = -\frac{\partial \psi}{\partial x} \tag{5}$$

equations (1)–(4) can be rewritten as

$$\frac{D\zeta}{Dt} = \frac{g}{\bar{\rho}_0}\frac{\partial \rho}{\partial x} + A_h\frac{\partial^2 \zeta}{\partial x^2} + A_v\frac{\partial^2 \zeta}{\partial z^2} \tag{6}$$

$$\frac{D\rho}{Dt} = \frac{\partial \psi}{\partial x}\frac{\partial \rho_0}{\partial z} \tag{7}$$

$$\nabla^2 \psi = \zeta \tag{8}$$

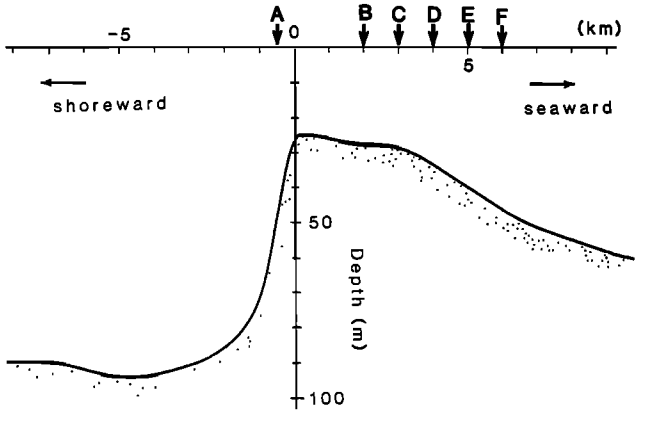

Fig. 2. The bathymetric cross section of Stellwagen Bank along line *G-H* in Figure 1. The arrows indicate the locations where the calculated vertical displacements of the isopycnal lines are decomposed into a series of normal modes (see Figure 13).

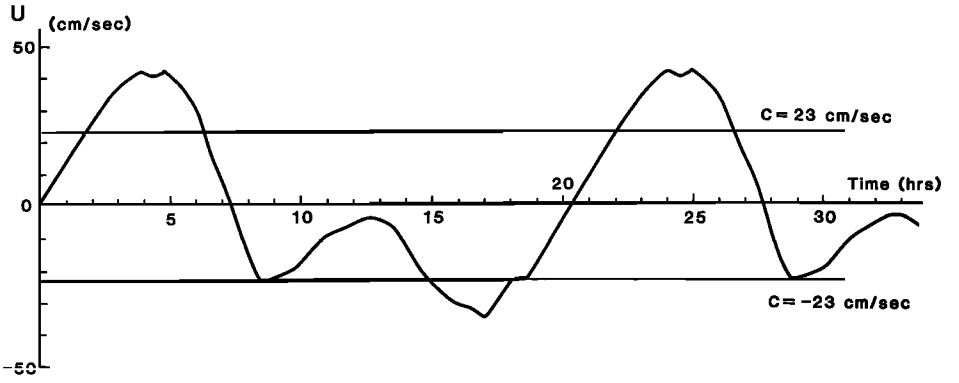

Fig. 3. The cross-bank component of the barotropic tidal flow velocity observed over the bank crest. The phase velocity of the first-mode internal wave over the bank crest is also shown.

where ∇^2 is the Laplacian operator, $\nabla^2 = \partial^2/\partial x^2 + \partial^2/\partial z^2$. Numerical simulation is made by integrating equations (6)–(8) with suitable initial and boundary conditions. For this purpose, equations (6)–(8) are replaced with a finite difference scheme by applying the centered difference and leapfrog scheme with a time increment Δt. In particular, the Arakawa Jacobian is used for an expression of the advective term [*Arakawa*, 1966].

The horizontal extent of the numerical model is $-50 \leq x \leq 50$ km, whereas the vertical extent is $0 \leq z \leq 90$ m. Stellwagen Bank is assumed to be situated in the region of $-2.5 \leq x \leq 10$ km connecting with the flat bottom of 90-m depth shoreward ($-50 \leq x \leq -2.5$ km) and 62.5-m depth seaward ($10 \leq x \leq 50$ km). This domain is divided into rectangular grids with a horizontal spacing of 250 m and a vertical spacing of 2.5 m. In this grid system, ψ is specified at each grid point, and ρ is specified at the center of four neighboring grid points.

The basic vertical density profile $\rho_0(z)$ is approximated as is shown in Figure 4, where the upper and lower mixed layers are separated by the linear density stratification assumed over a depth range of 5 to 50 m. For this model stratification, the phase velocities of the first- and second-mode internal waves over the bank crest are calculated as 23 and 11.1 cm/s, respectively. These values agree well with those calculated for the observed stratification, specifically, 23 and 10.5 cm/s [*Chereskin*, 1983].

The top and bottom surfaces of the stratified fluid are hypothesized as rigid. Furthermore, the inflow and outflow of the barotropic tide are specified at the lateral open boundaries such that the observed barotropic tidal flow velocity (see Figure 3) is reproduced at the bank crest. As a result, the top and bottom boundary conditions are expressed in terms of ψ as

$$\begin{aligned} \psi &= 0 \qquad z = -h(x) \\ \psi &= Q(t) \qquad z = 0 \end{aligned} \tag{9}$$

where $z = -h(x)$ is the equation of the bottom, and the barotropic tidal volume flux $Q(t)$ is determined from the data at the bank crest (depth of 27.5 m) shown in Figure 3. It should be noted that in this numerical model, the time variation of the tidal flow occurs completely in phase throughout the entire domain owing to both the rigid top approximation and the incompressibility assumption. This is permissible because we are concerned only with the internal wave generation region directly over the bank with a horizontal length scale of about 10 km, and the phase of the barotropic tidal flow varies only slightly over this distance. Since only the barotropic tidal flows are specified at the lateral open boundaries, the internal waves emanated from the bank are reflected back into the calculation region. For this reason, we shall be concerned only with the calculated wave field over the bank until about 30 hours from the onset of motion (see Figure 3) in which the effect of these reflected internal waves is not included.

With the assumption that $A_h = 10$ cm^2/s and $A_v = 20$ cm^2/s, the numerical computation proceeds from an initial state of rest with a time step of 2 min. First, the spatial distributions of ζ and ρ at each time step are predicted from equations (6) and (7). Then the spatial distribution of ψ at the specified time step is obtained from the corresponding spatial distribution of ζ by solving equation (8) iteratively. In order to avoid numerical instability, the Euler-backward scheme is applied every 20 time steps.

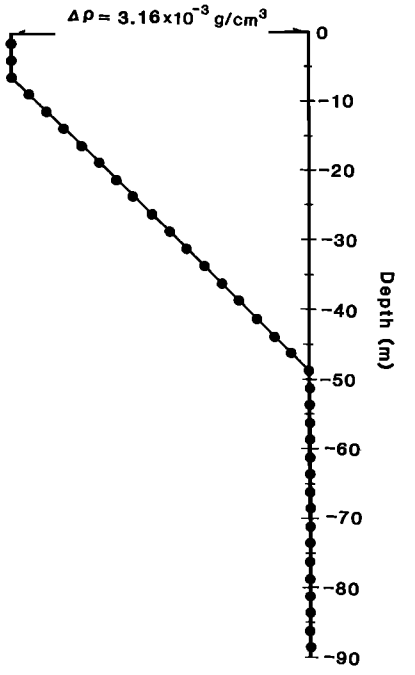

Fig. 4. The vertical density stratification assumed in the numerical simulation.

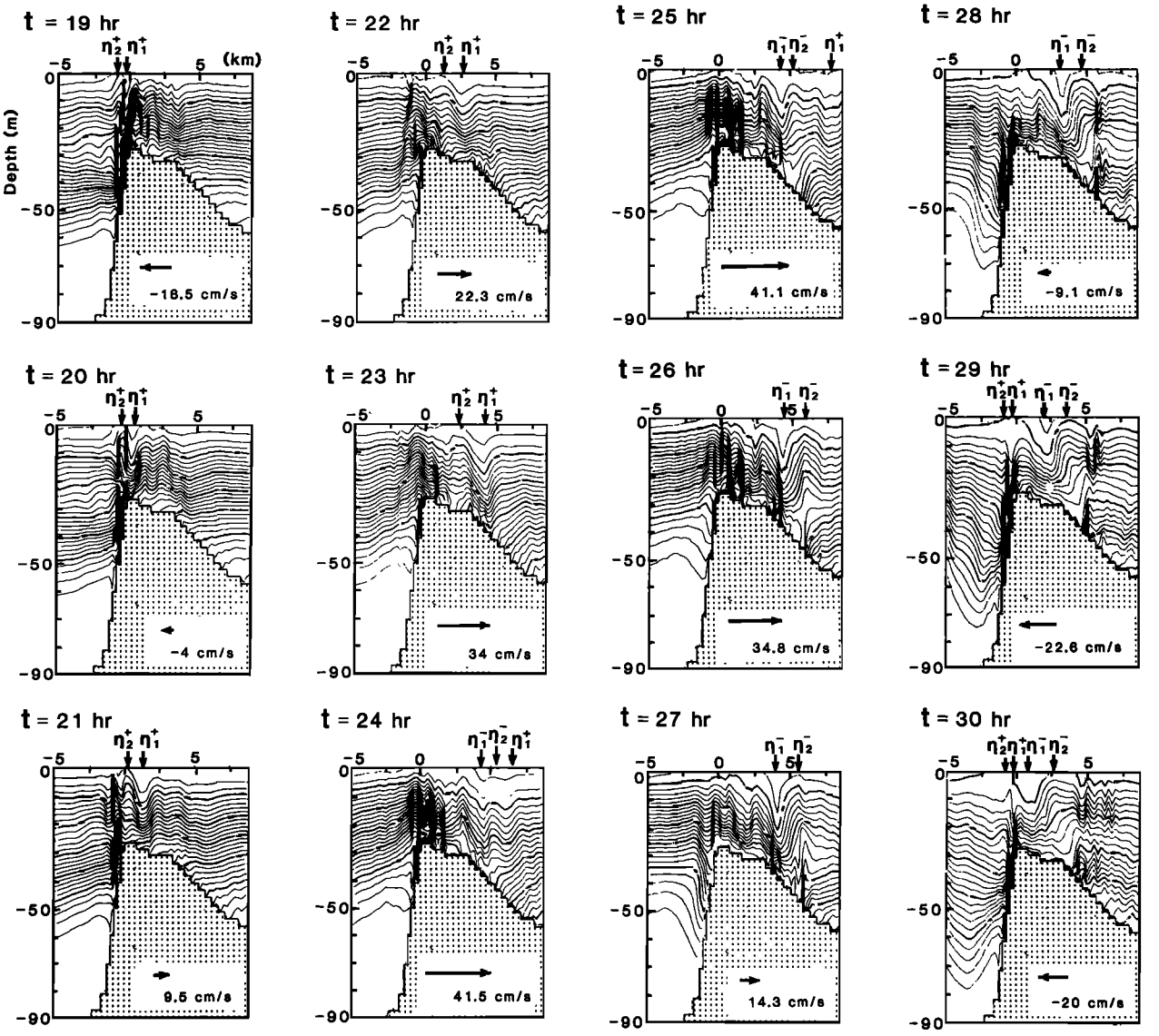

Fig. 5. The calculated result of the internal wave generation process over the bank during part of the second tidal cycle (see Figure 3). The symbols η_1^+ and η_2^+ show the seaward propagating first- and second-mode internal waves respectively, whereas η_1^- and η_2^- show the shoreward propagating first- and second-mode internal waves, respectively. The numeral and arrow at the bottom of each figure indicate the magnitude and direction of the barotropic tidal flow over the bank crest.

4. RESULTS

The calculated time development of the internal waves over the bank during part of the second tidal cycle (see Figure 3) is shown in Figure 5. In this section, we briefly describe the calculated result, checking it via a comparison with several acoustic images obtained by *Chereskin* [1983].

In the calculated result at $t = 19$ hours, the isopycnal displacements which occur in phase between the upper and lower layers can be seen immediately shoreward of the bank crest (this feature suggests a first-mode response, denoted as η_1^+), with the neighboring ones occurring out of phase between the upper and lower layers (this feature suggests a second-mode response, denoted as η_2^+). As the flood tidal flow decreases, η_1^+ and η_2^+ leave the shoreward slope successively ($t \simeq 20$ hours) and thereafter propagate seaward in the reversed (ebb) tidal flow. At the same time, the isopycnals over the shoreward slope are gradually elevated as the ebb tidal flow increases. The comparison of the calculated result with the acoustic image at $t = 23.3$ hours is shown in Figure 6. We can see in the acoustic image that the band of acoustic reflectors is elevated immediately shoreward of the bank crest and about 3 km seaward of the bank crest, in agreement with the calculated result.

As the ebb tidal flow further increases and hence approaches the maximum ($t \simeq 24$ hours), the isopycnals over the seaward slope begin to be displaced; the isopycnals about 4.5 km seaward of the bank crest are depressed both in the upper and lower layers (this feature suggests a first-mode response, denoted as η_1^-), whereas the neighboring ones about 6 km seaward of the bank crest are elevated in the upper layer and are depressed in the lower layer (this feature suggests a second-mode response, denoted as η_2^-). For the next few hours, the ebb tidal flow nearly keeps its maximum value. As is clearly seen in Figure 5, η_1^- and η_2^- are significantly amplified during this period, staying at the same locations. With the relax of the ebb tidal flow at $t \simeq 26$ hours, η_1^- and η_2^- begin to move shoreward. At the same time, the isopycnal elevation over the shoreward slope is gradually reduced as the

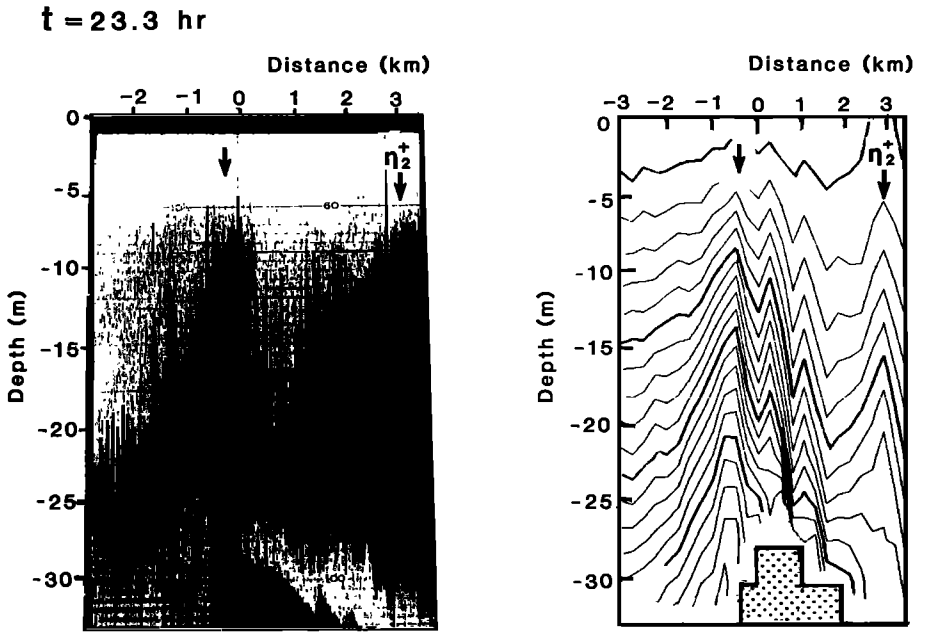

Fig. 6. Comparison of the calculated result with the acoustic image [*Chereskin*, 1983] at $t = 23.3$ hours.

ebb tidal flow decreases. Figure 7 shows the comparison of the calculated result with the acoustic image at $t = 28$ hours, shortly after the tidal flow reversal. Although the acoustic image over the shoreward slope is not clear, we can see that the band of acoustic reflectors is depressed about 3 km seaward of the bank crest and is elevated about 5 km seaward of the bank crest. These features are interpreted as being due to η_1^- and η_2^-, respectively.

Thereafter, η_1^- and η_2^- continue to propagate shoreward in the reversed (flood) tidal flow. Simultaneously, as the flood tidal flow approaches the maximum, the isopycnal displacements which occur in phase between the upper and lower layers begin to be formed again immediately shoreward of the bank crest, with the neighboring ones occurring out of phase between the upper and lower layers. The propagation of η_1^- and η_2^- is noticed in the acoustic image at $t = 29.5$ hours (Figure 8), where the depression and elevation of the band of acoustic reflectors are seen seaward of the bank crest by about 1 and 3 km respectively, in agreement with the calculated result. At $t = 30.5$ hours, η_1 comes over the shoreward slope and positively interferes with the isopycnal depression there. The comparison of the calculated result with the acoustic image is shown in Figure 9. As is reproduced in the calculated result, the band of acoustic reflectors immediately shoreward of the bank crest is seen to be significantly depressed.

Although the complete comparison between the calculated results and the acoustic images cannot be made since the acoustic images cover only a depth range from the surface down to about 30 m, general features acoustically observed are well reproduced in the calculated results. In the next section, therefore, the generation mechanism for these internal waves is investigated through a physical interpretation of the calculated results.

5. DISCUSSION

In an earlier paper [*Hibiya*, 1986], the author analytically discussed the generation mechanism of internal waves by a relatively strong tidal flow over a sill. It was shown that an

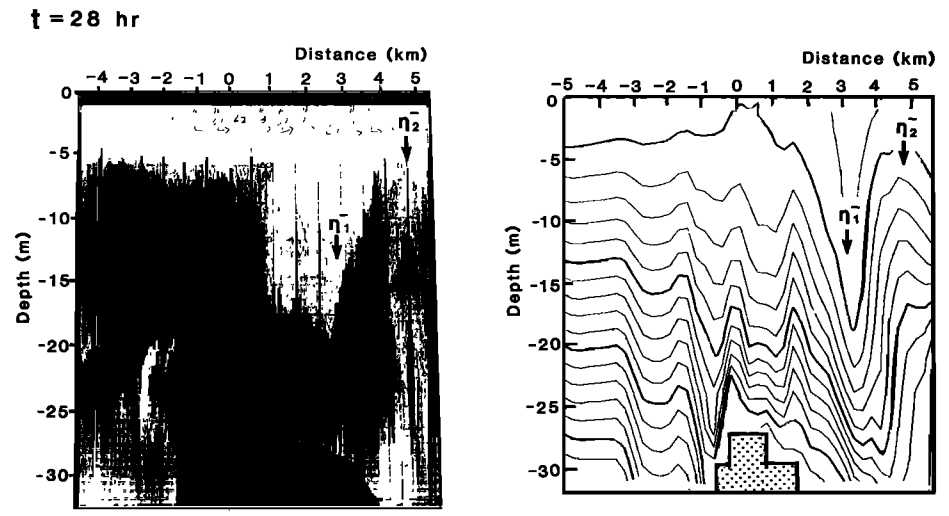

Fig. 7. As in Figure 6 but for $t = 28$ hours.

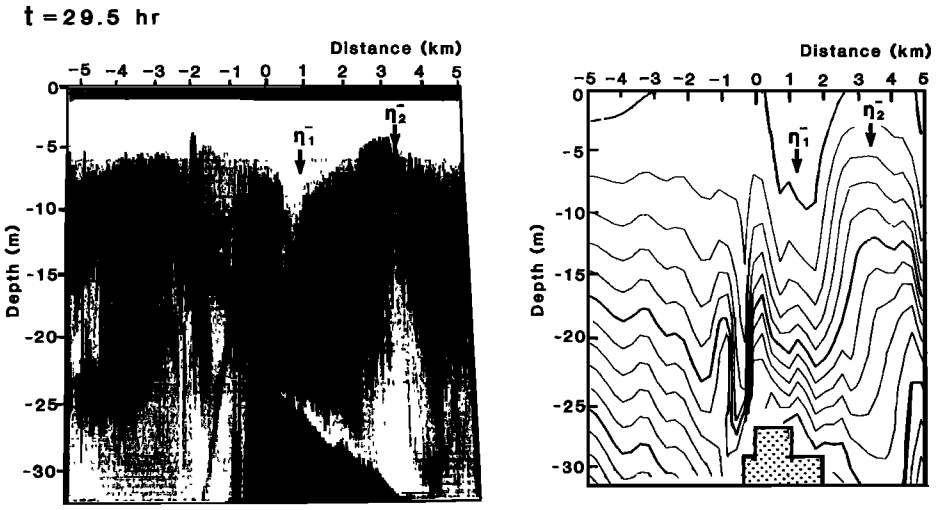

Fig. 8. As in Figure 6 but for t = 29.5 hours.

internal wave with an upstream phase propagation is gradually formed through the interference among infinitesimal-amplitude internal waves (elementary waves) emanated from the sill at each instant of time. Furthermore, the propagation of these elementary waves was described by use of characteristics, and several time dependent features were demonstrated. Unfortunately, because the theory presupposes linearized bottom boundary conditions, its quantitative applicability to the present case (a large-amplitude topography) is largely limited. Nevertheless, bearing in mind that the main purpose of this paper is to see whether or not the generation mechanism of internal waves can be qualitatively explained as a transient response of stratified fluid, we will apply the method of characteristics in a similar, yet slightly different fashion.

Since the tidal volume flux Q is assumed to be a function only of time, the barotropic tidal flow velocity over the bank is given by

$$U(x, t) = Q(t)/h(x) \tag{10}$$

where $h(x)$ is the water depth. Assuming the WKB type approximation, the equation of the characteristics for the ith-mode internal wave with a shoreward phase propagation is expressed as

$$\frac{dx}{dt} = U(x, t) - c_i(x) \tag{11}$$

and that for the ith-mode internal wave with a seaward phase propagation is expressed as

$$\frac{dx}{dt} = U(x, t) + c_i(x) \tag{12}$$

where c_i indicates the local phase velocity of the ith-mode internal wave. Since the first- and second-mode internal responses seem to be dominant in the calculated result, we henceforth confine our attention to the lowest two internal modes. The distribution of c_1 and c_2 over Stellwagen Bank for the density stratification assumed in the numerical simulation (see Figure 4) is shown in Figure 10. Using these data, a series of characteristics of the seaward and shoreward propagating elementary waves emanated from the bank slope regions at the time interval of Δt = 30 min are obtained as shown in Figures 11 and 12 respectively. Superimposed are the regions in which the tidal flow becomes supercritical with respect to

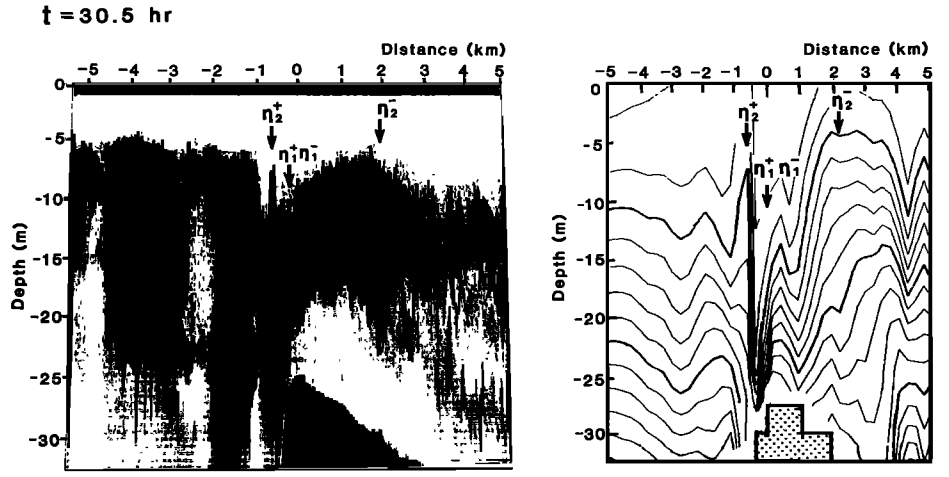

Fig. 9. As in Figure 6 but for t = 30.5 hours.

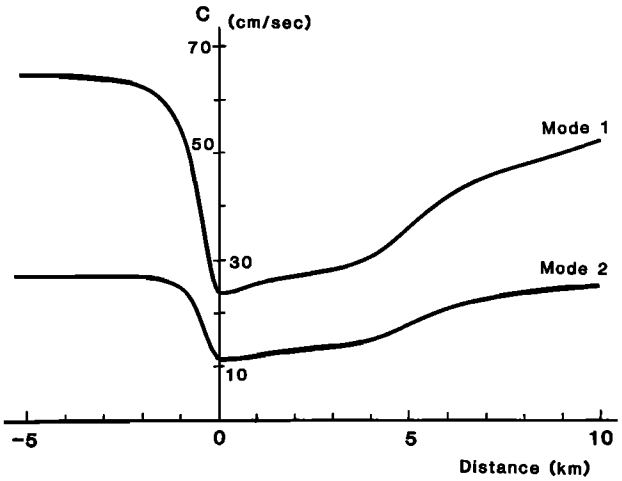

Fig. 10. The distribution of phase velocities of the first- and second-mode internal waves over the bank for the density stratification assumed in the numerical simulation (see Figure 4).

each internal mode ($-U/c_i > 1$, $i = 1, 2$). Furthermore, in order to see whether the result of the numerical simulation is qualitatively explained in terms of this theoretical analysis, calculated vertical displacements of isopycnal lines $\eta(z, t)$ at various horizontal locations are decomposed into a series of normal modes as

$$\eta(z, t) = \sum_n A_n(t) Z_n(z) \tag{13}$$

where $Z_n(z)$ is the nth-mode vertical eigenfunction with its maximum value normalized to unity. For reference purpose, $A_1(t)$ and $A_2(t)$ at the selected six locations, A–F (see Figure 2), are shown in Figure 13 together with the corresponding vertical eigenfunctions.

5.1. *Generation Mechanism of the Seaward Propagating Internal Waves*

During the early phase of the flood when the tidal flow is subcritical ($-U/c_i < 1$, $i = 1, 2$) throughout the entire region over the bank, the characteristics emanated from the bank slope regions propagate upstream without bunching. However, as the flood tidal flow increases and hence a region in which it becomes supercritical ($-U/c_i > 1$, $i = 1, 2$) is gradually formed, the characteristics of each internal mode encountered by this region begin to be carried downstream toward the location where the tidal flow becomes critical ($-U/c_i = 1$, $i = 1, 2$; hereinafter referred to as "critical locations"). As is seen in Figure 11, the critical locations with respect to the first and second modes during the flood phase are somewhat independent of time and are shoreward of the bank crest by about 0.25 and 0.5 km, respectively. It follows that the characteristics emanated from the shoreward slope bunch in the vicinity of these locations (see Figure 11), indicating that the first- and second-mode internal waves are gradually amplified there. With the decrease of the flood tidal flow, the closely bunched characteristics of the first and second mode leave the shoreward slope at $t \simeq 19.5$ and 20.5 hours, respectively, and thereafter propagate seaward in the reversed (ebb) tidal flow.

This theoretical result provides qualitatively consistent explanations for the time dependent features of generation and propagation processes of η_1^+ and η_2^+ revealed in the numerical simulation (see Figure 5). The time histories of $A_1(t)$ and $A_2(t)$ at location A are shown in Figure 13. This location is about 0.5 km shoreward of the bank crest and is very close to the critical location with respect to the second mode during the flood phase. We can see in this figure that the amplitude of the isopycnal displacement of each internal mode increases as the characteristics bunch over the shoreward slope (15 hr $\lesssim t \lesssim$ 17 hours) and begin to decrease as the bunched character-

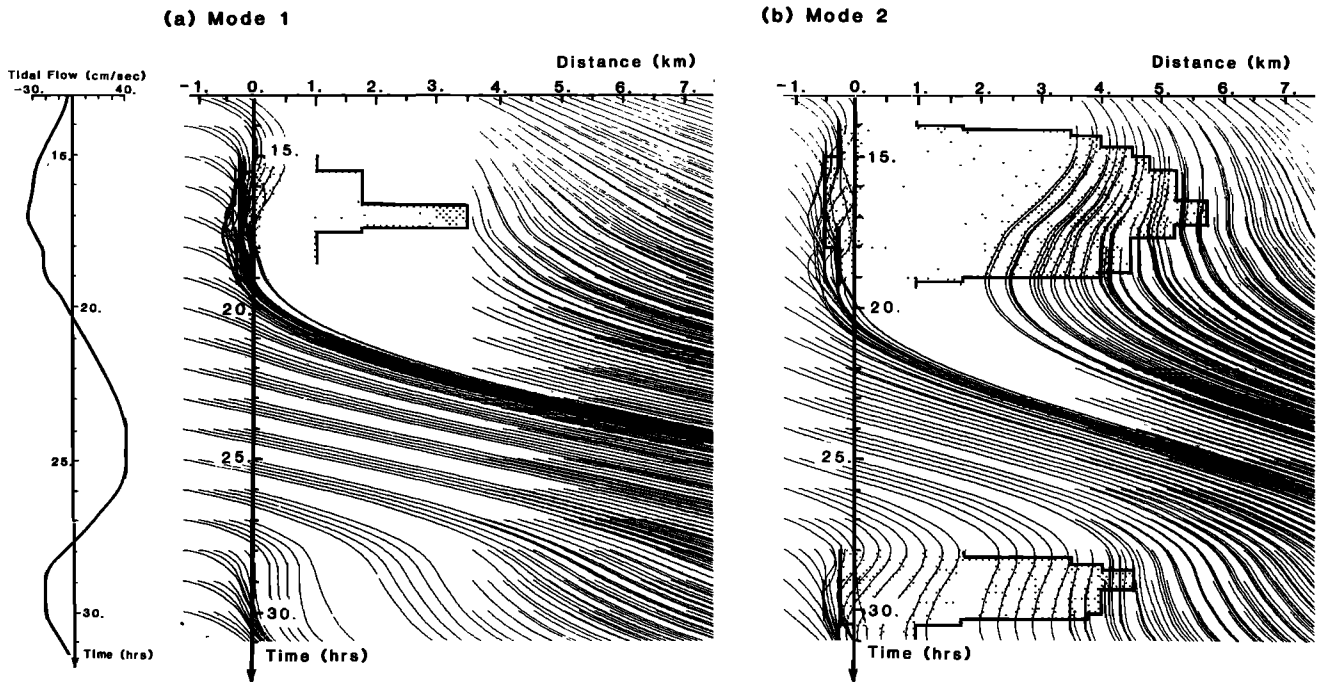

Fig. 11. A series of characteristics of the seaward propagating (*a*) first-mode and (*b*) second-mode internal waves emanated from the bank slope regions at the time interval of 30 min. The corresponding tidal flow condition is indicated at the left of the figure. Superimposed are the regions in which the tidal flow becomes supercritical with respect to each internal mode.

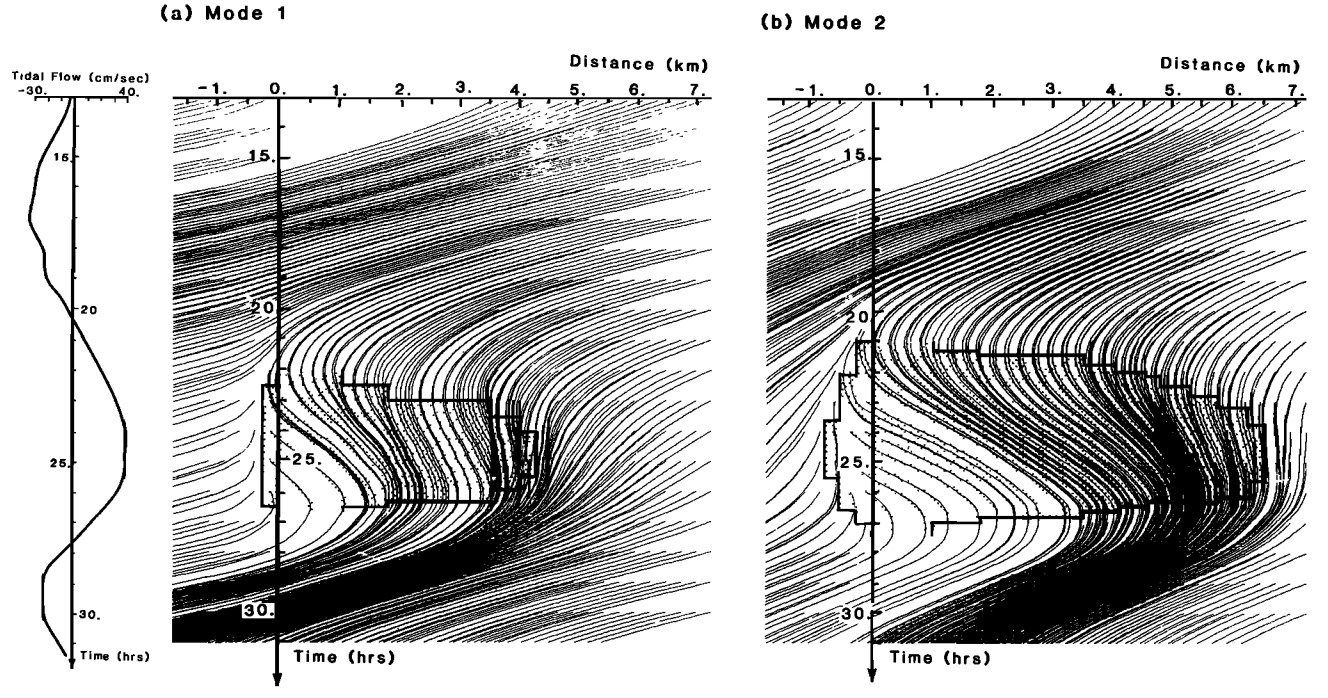

Fig. 12. As in Figure 11, but for the shoreward propagating internal waves.

istics leave this location ($t \simeq 18.5$ hours). As is shown in Figure 11, the bunched characteristics of the first mode pass locations *B*, *C*, *D*, *E*, and *F* (see Figure 2) at $t = 21.5$, 22.2, 22.8, 23.2, and 23.8 hours respectively, whereas those of the second mode pass locations *B*, *C*, *D*, and *E* at $t = 22.6$, 23.5, 24.0, and 24.5 hours, respectively. The time histories of $A_1(t)$ and $A_2(t)$ at locations *B*–*F* are shown in Figure 13. It is found that the rapid decrease of $A_1(t)$ due to η_1^+ and the increase of $A_2(t)$ due to η_2^+ at these locations occur simultaneously with the arrival of the bunched characteristics of each internal mode. This verifies the validity of the theoretical analysis by use of characteristics.

5.2. *Generation Mechanism of the Shoreward Propagating Internal Waves*

During the flood phase of the tidal flow, the characteristics emanated from the bank slope regions are advected away downstream without bunching. However as the tidal flow reverses and hence a region in which it becomes supercritical is gradually formed, the characteristics encountered by this region begin to be carried downstream toward the critical location where $-U/c_i = 1$ ($i = 1, 2$). As is shown in Figure 12, the critical locations with respect to the first and second modes move downstream as the ebb tidal flow increases. Since the ebb tidal flow becomes somewhat constant for a few hours after it reaches the maximum at $t \simeq 24$ hours, the characteristics of each internal mode eventually bunch in the vicinity of the location where $U_{max} = c_i$ ($i = 1, 2$), indicating that the first- and second-mode internal waves are gradually amplified there. With the relax of the ebb tidal flow ($t \simeq 26$ hours), the bunched characteristics of the first and second modes begin to propagate shoreward.

This theoretical result qualitatively explains the time dependent features of η_1^- and η_2^- revealed in the numerical simulation. Locations *E* and *F* (see Figure 2) are seaward of the bank crest by 5 and 6 km, respectively, and are close to the critical locations with respect to the first and second modes when the ebb tidal flow is maximum. It is clearly seen in Figure 13 that the amplitude of the isopycnal displacement of the first mode at location *E* and that of the second mode at location *F* gradually increase after the ebb tidal flow reaches the maximum, and hence the characteristics bunch in the vicinity of these locations (24 hours $\lesssim t \lesssim$ 26 hours). As is shown in Figure 12, the bunched characteristics of the first mode pass locations *D*, *C*, and *B* at $t = 27.2$, 28.2, and 29 hours, respectively, whereas those of the second mode pass locations *E*, *D*, and *C* at $t = 27.5$, 28.8, and 29.4 hours, respectively. This is consistent with the calculated result shown in Figure 13 where the rapid decrease of $A_1(t)$ due to η_1^- and the increase of $A_2(t)$ due to η_2^- at these locations are found to occur simultaneously with the arrival of the bunched characteristics of each internal mode.

6. SUMMARY AND CONCLUDING REMARKS

In the present study, the generation mechanism of internal waves by a relatively strong tidal flow over a large amplitude topographic feature has been investigated by taking the case of Stellwagen Bank as an example.

First, a numerical simulation of the internal wave generation over the bank during the field study by *Chereskin* [1983] was carried out, and the continuous generation process which is consistent with the acoustic images obtained at several stages of the tidal flow has been demonstrated. Next, in order to understand the time dependent features shown in the calculated result, a theoretical investigation was made using the characteristics which describe the propagation of the first- and second-mode internal waves [*Hibiya*, 1986]. This analysis has shown that each mode internal wave with an upstream phase propagation is efficiently amplified while being carried downstream toward the location where the maximum tidal flow becomes critical; with the relaxation of the tidal flow, the internal wave thus amplified begins to propagate upstream.

In previous studies, tidally generated internal waves over Stellwagen Bank were interpreted as quasi-steady lee waves

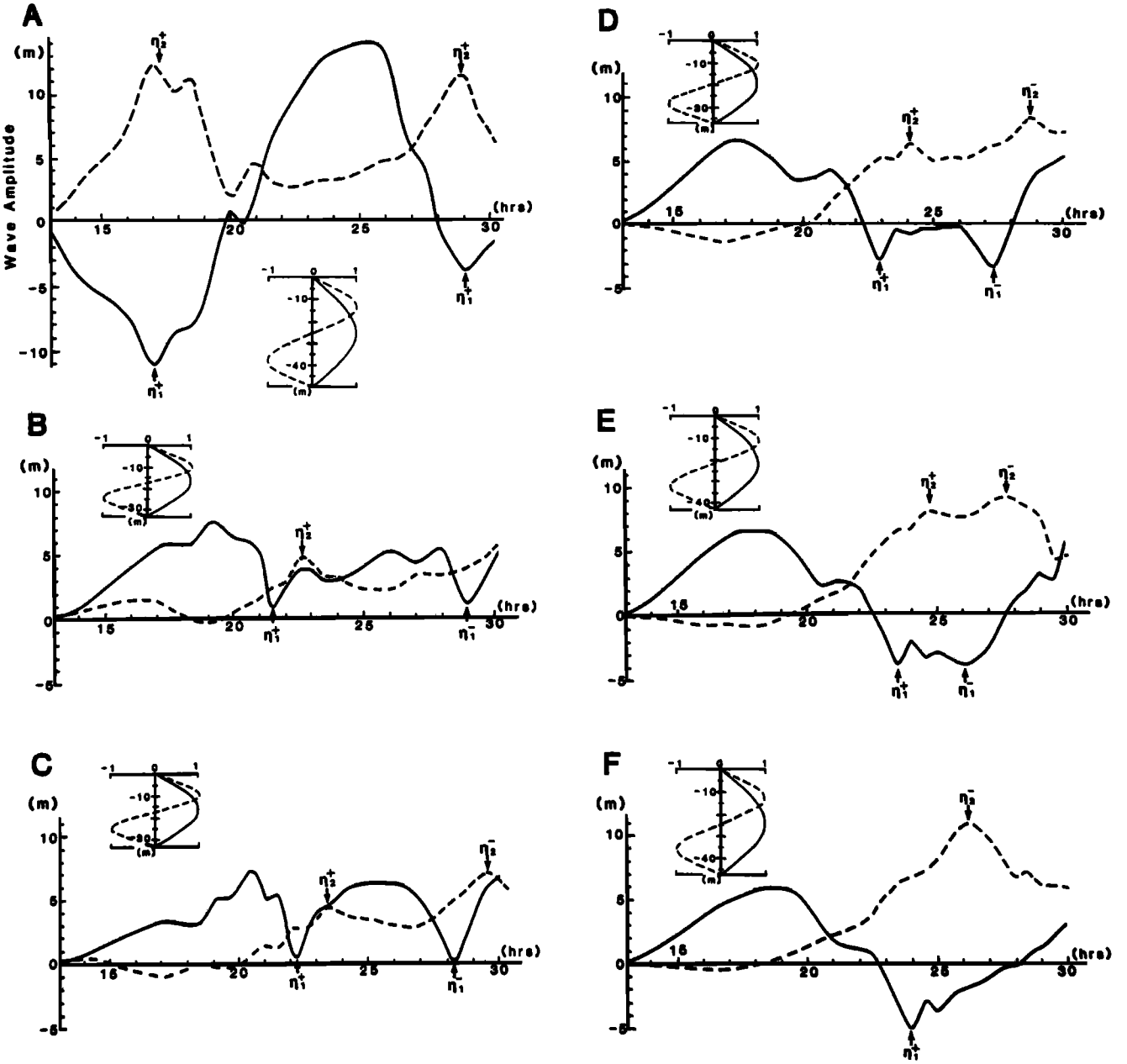

Fig. 13. The time histories of the amplitude of the first- and second-mode isopycnal displacements at locations *A-F* over the bank (see Figure 2). The corresponding vertical eigenfunctions at each location are also shown.

[*Haury et al.*, 1979; *Chereskin*, 1983]. However, from the consistency between the calculated and theoretical results obtained in the present study, it can be concluded that these internal waves are not quasi-steady lee waves, but transient waves formed in response to a time-varying tidal flow.

Although the physical mechanism for the tidal generation of internal waves has thus been qualitatively clarified, there remain some problems to be investigated before our understanding of this phenomenon becomes complete. For example, the internal wave reflection and upstream blocking of the stratified flow due to the steep slope of the bottom topography as well as the nonlinear evolution of internal waves during the course of propagation must also be considered. Further laboratory and numerical studies together with detailed field observations are necessary before a theory which incorporates these factors can be developed.

Acknowledgments. The author expresses his gratitude to K. Kajiura of the Earthquake Research Institute, University of Tokyo, for critical reading of the manuscript. He also expresses his gratitude to T. Matsuura of Ibaraki University for helpful discussions.

REFERENCES

Arakawa, A., Computational design for long-term numerical interpretation of the equations of fluid motion: Two-dimensional incompressible flow, I, *J. Comput. Phys.*, *1*, 119–143, 1966.

Chereskin, T. K., Generation of internal waves in Massachusetts Bay, *J. Geophys. Res.*, *88*, 2649–2661, 1983.

Farmer, D. M., and J. D. Smith, Tidal interaction of stratified flow with a sill in Knight Inlet, *Deep Sea Res., Part A*, *27*, 239–254, 1980.

Halpern, D., Observation on short internal waves in Massachusetts Bay, *J. Mar. Res.*, *29*, 116–132, 1971.

Haury, L. R., M. G. Briscoe, and M. H. Orr, Tidally generated internal wave packets in Massachusetts Bay, *Nature*, *278*, 312–317, 1979.

Haury, L. R., P. H. Wiebe, M. H. Orr, and M. G. Briscoe, Tidally generated high-frequency internal wave packets and their effects on plankton in Massachusetts Bay, *J. Mar. Res.*, *41*, 65–112, 1983.

Hibiya, T., Generation mechanism of internal waves by tidal flow over a sill, *J. Geophys. Res.*, *91*, 7697–7708, 1986.

Lansing, F. S., and T. Maxworthy, On the generation and evolution of internal waves, *J. Fluid Mech.*, *145*, 127–149, 1984.

Maxworthy, T., A note on the internal solitary waves produced by tidal flow over a three-dimensional ridge, *J. Geophys. Res.*, *84*, 338–346, 1979.

T. Hibiya, Earthquake Research Institute, University of Tokyo, 1-1 Yayoi, Bunkyo-ku, Tokyo 113, Japan.

(Received July 30, 1987;
accepted September 29, 1987.)